Extreme Mechanics Letters 20 (2018) 14–20

Contents lists available at ScienceDirect

Extreme Mechanics Letters

journal homepage: www.elsevier.com/locate/eml

Design of piezoMEMS for high strain rate nanomechanical experiments

Rajaprakash Ramachandramoorthy [a,b,1], Massimiliano Milan [a,d,1], Zhaowen Lin [a,b], Susan Trolier-McKinstry [c], Alberto Corigliano [d], Horacio Espinosa [a,b,*]

[a] Department of Mechanical Engineering, Northwestern University, Evanston, IL – 60208, USA
[b] Theoretical and Applied Mechanics Program, Northwestern University, Evanston, IL – 60208, USA
[c] Department of Materials Science and Engineering and Materials Research Institute, Pennsylvania State University, University Park, PA – 16802, USA
[d] Department of Civil and Environmental Engineering, Politecnico di Milano, 20133 Milano, Italy

ARTICLE INFO

Article history:
Received 7 October 2017
Received in revised form 21 November 2017
Accepted 21 December 2017
Available online 1 January 2018

ABSTRACT

Nanomechanical experiments on 1-D and 2-D materials are typically conducted at quasi-static strain rates of 10^{-4}/s, while their analysis using molecular dynamic (MD) simulations are conducted at ultra-high strain rates of 10^{6}/s and above. This large order of magnitude difference in the strain rates prevents a direct one-on-one comparison between experiments and simulations. In order to close this gap in strain rates, nanoscale actuation/sensing options were explored to increase the experimental strain rates. Using a combination of COMSOL multiphysics finite element simulations and experiments, it is shown that thermal actuation, which uses structural expansion due to Joule heating, is capable of executing uniaxial nanomechanical testing up to a strain rate of 10^{0}/s. The limitation arises from system inertia and thermal transients. In contrast, piezoelectric actuation can respond in the GHz frequency range. However, given that the piezoelectric displacement is limited in range, a sagittal displacement amplification scheme is examined in the actuator design, which imposes a lower frequency limit for operation. Through a combination of analytical calculations and COMSOL dynamic analysis, it is shown that a piezoelectric actuator along with a displacement amplifier is capable of achieving ultra-high strain rates of $\sim 10^{6}$/s during nanomechanical testing.

1. Introduction

Recently, nanomaterials such as nanowires, nanotubes and nanoribbons are being exploited in applications such as high frequency resonators [1] and nanomechanical switches [2,3], which operate in the kHz–GHz regime. This requires their material properties to be characterized at high frequencies, in order to provide correct data for input into finite element models of the devices. Also, from a theoretical standpoint it is vital to gain insight into nanomaterials at a wide range of strain rates.

In the past two decades, research on experimental nanomechanics has focused on obtaining the properties of a variety of nanomaterials from metallic nanowires to carbon based 1-D and 2-D materials, e.g., nanotubes, graphene and more recently, to transition metal dichalcogenides (TMDC) [4–6]. The most common experiments used to explore the nanomechanical properties of these materials, are atomic force microscopy (AFM) [7,8] and nanoindentation [9], while micro-electromechanical systems (MEMS) based testing platforms [5,10,11] have been used for exploring material properties via *in situ* electron microscopy. These experimental efforts typically reveal size-effects, while strain rate effects, especially at strain rates beyond 0.01/s remain largely unexplored experimentally [12,13]. The main reason for the lack of nanoscale experiments at high strain rates is the requirement of fast actuation systems and concurrent fast response load cells with nano-Newton resolution. Nanoindentation has been used previously in the literature to conduct compression tests on sub-micron scale pillars at a strain rate of $\sim$0.1/s. But for achieving higher strain rates, MEMS based testing platforms offer a combination of fast actuation speeds, due to their low mass, and fast response capacitive load cells based on electronic sensing [10].

The strain rate dependent behaviors of nanomaterials have been explored extensively using simulations, such as molecular dynamics (MD) and dislocation dynamics (DD). These computational tools are typically used to obtain a "qualitative" understanding of the deformation mechanisms in nanomaterials, as the quantitative results vary significantly depending on the chosen interatomic potential or force field [14].

* Corresponding author at: Department of Mechanical Engineering, Northwestern University, Evanston, IL – 60208, USA.
E-mail address: espinosa@northwestern.edu (H. Espinosa).
[1] These authors contributed equally to this work.

https://doi.org/10.1016/j.eml.2017.12.006

The paper begins by reporting atomistic high strain rate simulations of single crystal silver nanowires to illustrate and motivate the need for developing high strain rate testing platforms that can unambiguously identify nanomaterials' mechanical properties. These experiments will be eventually used to test and validate available MD force fields. Two different actuation methods, namely thermal and piezoelectric, that can be implemented in MEMS platforms for testing 1-D and 2-D nanomaterials at high strain rates, were considered. A combination of COMSOL multiphysics finite element modeling (FEM), experiments, and analytical modeling were used to analyze the capabilities of these actuation methods for conducting high strain rate nanomechanical testing. We find that the thermal actuator is capable of actuating at speeds up to 10 μm/s, which translates to a strain rate of $\sim$3/s for a nanowire with gage length of 3 μm. On the other hand, piezoelectric actuation is capable of applying strain rates of $\sim 10^6$/s to a nanowire of similar gage length.

2. Molecular dynamic simulations and its shortcomings

In order to predict the mechanical properties of materials, typical MD simulations use interatomic potentials that simplify the system to pair-wise interactions. In the case of metallic nanomaterials, MD simulations are typically conducted using the Embedded Atom Method (EAM). For example, the EAM potential developed by Foiles et al. [15] was applied to three different families of crystalline silver nanowires to ascertain their mechanical properties at an ultra-high strain rate of 10^8/s, as shown in Fig. 1(a). The EAM based potentials include many-body interactions; hence they are capable of differentiating between atoms in the surface and the bulk. These EAM potentials are developed using a combination of pair-wise interactions and an embedding function. Typically, the pair-wise interactions are parameterized to recover bulk properties such as lattice constants, elastic constants and stacking fault energies. The embedding function, on the other hand, is obtained from first principle calculations such as density functional theory [15]. Given that these EAM potentials can only be fit to a limited number of experimental data, they may not be able to capture the entire phase space, and eventually this leads to some shortcomings. Specifically, for the case of metallic nanowires, different potentials result in different yield strain deformation and hardening mechanisms [16]. Research shows that key intrinsic properties leading to more accurate predictions of yield and plastic behavior of metals are the intrinsic stacking fault energy, which determines the width of dislocation dissociation, and the unstable stacking fault energy, which can be viewed as the activation barrier that should be overcome when an intrinsic stacking fault is created [17]. These properties are used for the parameterization of various potentials. For example, as shown in Fig. 1(b), when different EAM potentials are applied to the same bicrystalline nanowire tested in tension, the results varied in the predicted yield stress, yield strain, and the subsequent plasticity behavior. Therefore, a method of validating these EAM potentials needs to be established. Due to computational limitations, the strain rates achievable in atomistic simulations of nanostructures are on the order of 10^6/s or higher [18]. By contrast, strain rates achieved in experiments typically do not exceed 10^0/s. Thus, till now a true one-to-one comparison between experiments and MD simulations has not been possible, motivating examination of experimental platforms that can close this gap in knowledge. To circumvent this limitation, MD results are typically extrapolated using rate-dependent thermodynamic models based on the activation energy required to drive the process of interest [19]. The energy landscape is computed via atomistic simulations and then employed to extrapolate behavior at slower strain rates [20]. For example, classical dislocation nucleation theory [18,21] has been used to extrapolate MD simulation results to experimental yield stresses [10].

On the other hand, parallel replica dynamics [22] replicates the original configuration of the system on multiple processors and monitors for the first transition event. Once a processor detects an event, all the processors are stopped and the simulation clock is advanced by the sum of the trajectory times accumulated by all the replicas from the beginning. Then, on the one processor where the transition event occurred, the replica is integrated forward for a specific pre-chosen time, so that new transitions may occur. This replica becomes the new configuration of the system and the entire protocol is repeated. This method thus extends the MD time scales with high-efficiency. Unfortunately, this method has been used only for ultra-small systems with a few hundred atoms, as the transitions become too frequent in larger systems [23]. Thus, our aim is to provide the means for development of a "quantitative" force field and means for validating theoretical models of defect nucleation [10,24].

3. MEMS with thermal actuation — strain rates up to 1/s

A typical MEMS nanomechanical testing platform consists of an actuator, a load sensor and a 1-D/2-D sample of interest, which is mounted in-between the actuator and the load sensor [27]. The fast response load detection is typically accomplished using capacitance based sensing as discussed in detail elsewhere [28]. The key challenge in these tests is providing a controlled actuation motion at the nanometer range. A variety of actuation methods has been reported in the literature including, thermal, electrostatic and magnetic approaches [10,29,30]. Thermal actuation with its high-force and large-displacement capability [31], is a reliable and stable method to conduct quasi-static testing of a variety of materials such as nanotubes [6,27,32], nanowires [10,33] and thin films [34]. Thermal actuator beams are typically attached at a specific angle on both sides of a freestanding central shuttle, while the other end of the beams is fixed to the substrate [27]. When a voltage is applied to the beams, the current flow generates Joule heating, with commensurate thermal expansion and in turn central shuttle displacement [35]. As such, the thermal actuator generates an axial displacement to one end of the sample while the other end is connected to an interdigitated capacitive load sensor, whose stiffness is chosen to achieve a desired sample elongation. A more detailed explanation of the aforementioned testing concept with this MEMS platform is available elsewhere [36].

For high strain rate testing, the challenge is not only to produce controlled nanometer scale displacements, but also to achieve them at high speed. This requires a study of the voltage profiles applied to the actuator beams, such that a known time-varying displacement is applied to the sample by the thermal actuator. In the dynamic analysis, the mass of the thermal actuator beams, the heat sink beams (to avoid sample heating), and the central shuttle to which the nanowire is attached were considered. In order to achieve actuation at high speeds and increase the dynamic range of the system, the mass has to be kept as low as possible. The mass of the actuation system, employed in this study, was calculated using the density of silicon and the volume of the actuator as 21 μg. Using multiphysics finite element simulations, it was ascertained that the inherent low mass of the MEMS device allows actuation speeds of $\sim$10 μm/s, see Fig. 2(a). Above this speed, the system starts to lag behind the applied voltage due to inertia and rate-limiting heat transfer, as shown in Fig. 2(b).

In order to validate the simulations, experiments were conducted using a MEMS device with glued thermal actuator and load sensor shuttle such that the capacitive measurement could be used to detect the actuator displacement. The experimental measurement is shown in Fig. 2(c). Using the same voltage amplitude and different time histories, the thermal actuator was actuated at different speeds. As expected, due to dynamic effects, the thermal actuator lags beyond a speed of 10 μm/s as shown in Fig. 2(d). This speed translates to a strain rate of $\sim$2/s while testing nanowires of diameter $\sim$40 nm, with a gage length of $\sim$ 3 μm [10].

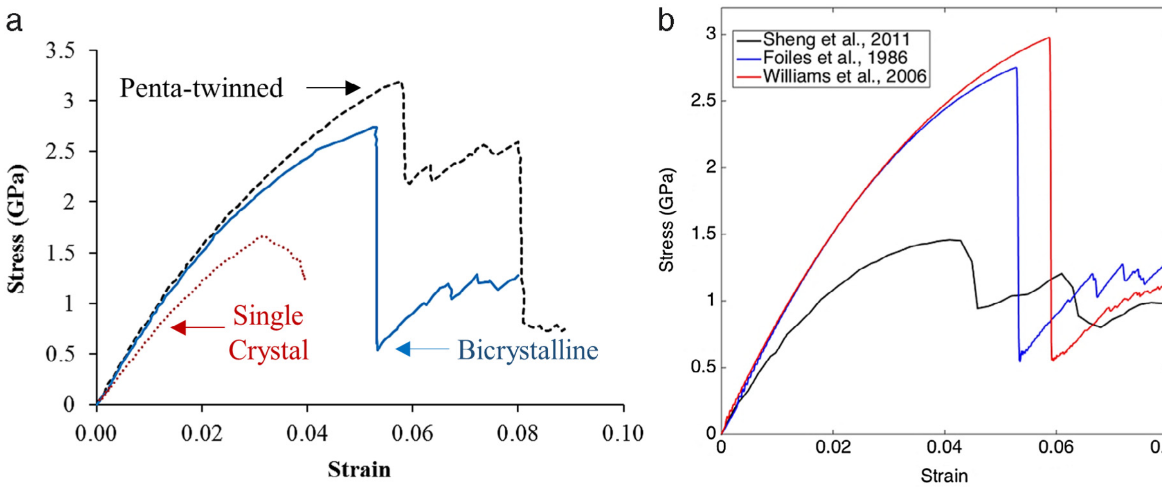

Fig. 1. (a) Tensile properties of three different silver nanowires penta-twinned, bicrystalline and single crystal explored using the EAM potential and (b) Stress–strain curves of bicrystalline nanowires obtained from MD simulations, using three different force fields [15,25,26].

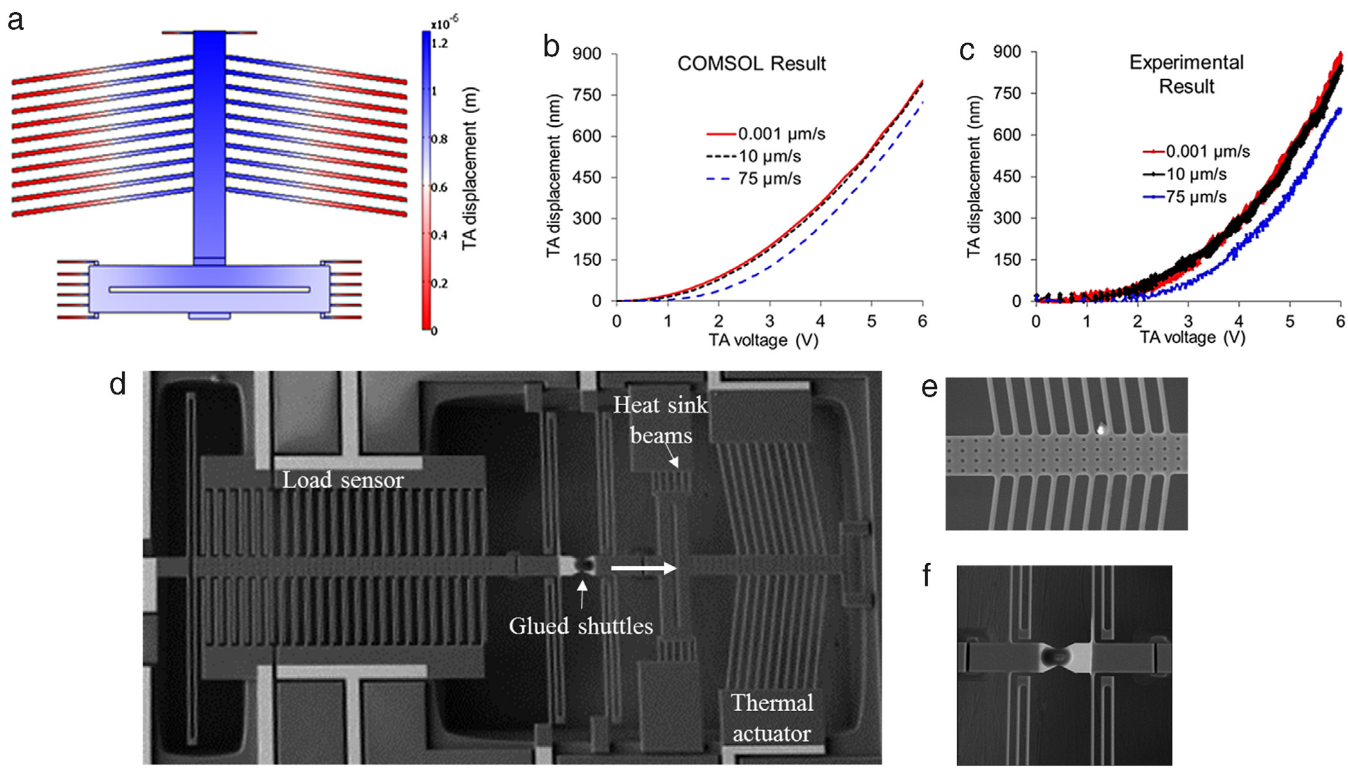

Fig. 2. (a) FEM model of the thermal actuator (TA) used in FEM multiphysics simulations. (b) Displacement as actuator increases at different speeds showing lag beyond 10 μm/s. (c) Experiments on MEMS device with glued actuator and sensor shuttles as shown in (d). Experiments confirmed that the system lags beyond 10 μm/s. (e) The shuttles of the thermal actuator with holes for mass reduction. (f) Magnified image of the glued shuttles.

4. MEMS with piezoelectric actuation — strain rates up to 10^6/s

In order to conduct experiments similar to the ultra-high strain rates used in MD simulations, a MEMS device with higher actuation speeds needs to be designed. Given that the piezoelectric crystals can respond to an applied field into the GHz frequency range [37,38] (albeit with progressively reduced amplitude as the various device resonance frequencies are exceeded), we hypothesized that using piezoelectric materials it is possible to design systems that can achieve high actuation speeds and high dynamic ranges. The actuation is based on the converse piezoelectric effect, namely, when a piezoelectric material is subjected to an electric potential difference, it deforms. The idea is to use such deformation to stretch the nanowire sample uniaxially. Piezoelectric actuation is already established as a method for achieving high dynamic response [39,40]. Other advantages of using piezoelectric thin-films for actuation are the high force and low input voltage. The typical piezoelectric materials previously used in MEMS fabrication are Aluminum Nitride (AlN) and Lead Zirconate Titanate (PZT) [39,41,42]. The AlN thin films are easy to fabricate and have a piezoelectric strain coefficient $d_{31,f}$ of ∼1.95 pm/V [39]. These films have been used previously in a multitude of actuators and sensors [43]. However, the deformation that is obtained, through the converse piezoelectric effect of AlN thin films, is insufficient for straining metallic nanowire samples to failure, for realistic film thicknesses. On the other hand, PZT thin films of 1 μm thickness have a much higher $d_{31,f}$ value of ∼30–50 pm/V [39], and thus are capable of producing larger deformations.

We began by studying the simplified piezoelectric system shown in Fig. 3. An 800 μm long PZT piezoelectric element is examined to ascertain if it is indeed capable of delivering the appropriate displacement required to deform metallic nanowires till failure. A typical strain needed to break a silver nanowire of 100 nm in diameter, with a gage length of ∼2 μm, can be ∼15%, taking into account both the elastic and plastic deformation. The simplified system considered here is a symmetric layered structure composed of a PZT thin layer (0.4 μm thickness), two platinum electrodes (0.1 μm thickness), one on the top and the other on the bottom of the piezoelectric material and finally, a support structure of SiO_2 layer (0.2 μm thickness) on top and bottom. The schematic of this simplified system's cross-section is shown in Fig. 3(a). Also, the nanowire was simulated as a fixed spring clamped on one end and the other end fixed to the piezoelectric system, see Fig. 3(b). The spring was simulated with the stiffness of a 100 nm diameter silver nanowire (k_{nw}).

Using the mechanical boundary conditions shown in Fig. 3(b), the FEM simulation result showed that with an applied voltage of 12 V, the maximum displacement obtained is 0.28 μm or a strain of 12% for a nanowire with a gage length of 2 μm. Such displacement would not be enough to strain metallic nanowires till failure. Thus, in order to increase the deformation obtained from the piezoelectric layer, we subsequently investigated a displacement amplification scheme, similar to the ones reported in the literature [42,44]. One of the typical amplification schemes used with piezoelectric actuators is flextensional actuators, including moonie and cymbal actuators [45]. In the moonie amplification scheme the displacement is amplified by flexural motion of the end caps attached to the top and bottom of the piezoelectric element [46]. On the other hand, in the cymbal amplification scheme the net displacement is a result of combination of flexural and rotational motions of the end caps [47]. It is also known that the piezoelectric actuators implemented with cymbal amplification schemes generate higher displacement and force compared to their moonie counterparts [45]. Thus, in this work we have designed an amplification scheme similar to the cymbal amplification scheme with flexural beams attached using hinges.

5. Piezoelectric actuator with displacement amplification scheme

The piezoelectric element shown in the previous section was embodied with a mechanical frame possessing hinges, such that displacement amplification can be achieved. A sagittal displacement amplifier was chosen for this purpose and its working principle is schematically shown in Fig. 4(a) [44,48]. The kinematic principle behind this sagittal amplification scheme is simple, the force applied to the side hinges by the piezoelectric actuator generates an amplified displacement in the vertical direction, as shown in Fig. 4(a). Under the assumption that the flexure hinges are pure rotational joints, an input displacement u_x translates into the amplified output displacement u_y. To derive an analytical expression, we assume that the four diagonal beams have infinite stiffness and the entire structure has one degree of freedom.

The amplification factor, 'a', is defined as the ratio between the vertical and the horizontal displacement, as shown in Fig. 4(a). From the kinematics shown, the ratio can be obtained using geometry as viz.,

$$a = \frac{u_y}{u_x} = \frac{\sin\left(\alpha'\right) - \sin\left(\alpha\right)}{\cos\left(\alpha\right) - \cos\left(\alpha'\right)} \tag{1}$$

where α is the initial diagonal beam angle and α' is the final diagonal beam angle. Since, $\delta = \alpha' - \alpha$, the difference between α' and α, is small, using first order Taylor approximation, Eq. (1) can be simplified to

$$\frac{u_y}{u_x} = \frac{\sin\left(\alpha'\right) - \sin\left(\alpha\right)}{\cos\left(\alpha\right) - \cos\left(\alpha'\right)} \approx \frac{\sin\left(\alpha\right) + \delta\cos\left(\alpha\right) - \sin\left(\alpha\right)}{\cos\left(\alpha\right) - \left[\cos\left(\alpha\right) - \delta\sin(\alpha)\right]} = \frac{1}{\tan\left(\alpha\right)} \tag{2}$$

In this simplified geometric model though, the compliances of the piezoelectric element and specimen are not included, which also influence the displacement and amplification ratios of the system. We account for such compliances in the following analytical formulation.

When a voltage is applied on the piezoelectric element, a force F is transmitted to the displacement amplifier through the joints B and B′, as shown in Fig. 4(a). Using typical force balance gives

$$\frac{k_{nw}u_y}{F} = \tan\left(\alpha'\right) \approx \tan\left(\alpha\right) \tag{3}$$

where k_{nw} is the stiffness of the nanowire. In the situation where the piezoelectric element has a finite stiffness k_p, the voltage-induced expansion u_x is affected due to the constraint from the frame. The actual expansion is reduced by F/k_p. Therefore, Eq. (2) becomes

$$\frac{u_y}{u_x - \frac{F}{k_p}} = \frac{1}{\tan\left(\alpha\right)} \tag{4}$$

Combining Eqs. (3) and (4), the amplification factor with the different stiffnesses accounted for is given by:

$$a = \frac{u_y}{u_x} = \frac{\tan\left(\alpha\right)}{\tan^2\left(\alpha\right) + \frac{k_{nw}}{k_p}} \tag{5}$$

Thus the amplification is a function of the stiffness of the nanowire. The vertical displacement u_y decreases as the nanowire stiffness increases. For example, a silver nanowire with a diameter of 100 nm and a length of 2 μm has a stiffness of $k_{nw} = 326$ N/m. A PZT beam with dimensions shown in Figs. 3(a) and 4(b) has a stiffness k_p of 15 000 N/m. Thus, $k_p \gg k_{nw}$, which simplifies Eq. (5) to Eq. (2).

Applying a voltage of 10 V between the electrodes, the horizontal displacement of the piezoelectric element u_x is 0.1 μm, identified using FEM multiphysics simulations. Employing an initial diagonal beam angle of 15°, the nanowire displacement is ∼746 nm. This displacement translates to a strain of ∼37.3% for a nanowire gage length of ∼2 μm, which is more than enough for tensile testing metallic nanowires till failure.

In order to validate the results obtained from the analytical calculations based on the simplified model and to understand the dynamic response of the system, a finite element analysis (FEA) was employed. The geometry shown in Fig. 4(b) was chosen for the piezoelectric actuator. The beams with low width form the hinges, to allow for the relative rotation between the piezoelectric element and the diagonal beams. Four movable diagonal beams were placed on each side to avoid a torsional movement of the shuttle resulting from a stiff nanowire potentially mounted at an off-centered position on the actuator shuttle. The moving structure is supported by multiple thin beams on all four corners and the nanowire is fixed on the moving shuttle. The 3D CAD model of the actuator was built using Rhinoceros software and subsequently imported into FEM multiphysics software to conduct non-linear dynamic analysis using a combination of solid mechanics and electrostatics.

As seen from Fig. 4(d), only half of the geometry is used in the FEM simulations, as this condition of symmetry allowed for faster analysis. The boundary conditions imposed on the model are A, A′, A′′: symmetry condition; B, B′, C: fixed; and C′: simple spring with displacement $= k_{nw}u_y$. In the FEM analysis, an electric field is

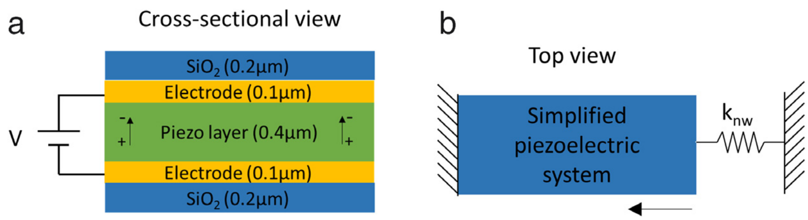

Fig. 3. (a) Schematic of the simplified piezoelectric system simulated in COMSOL FEM multiphysics software to ascertain the displacement range of the piezoelectric actuator. (b) Boundary conditions used in the simulation.

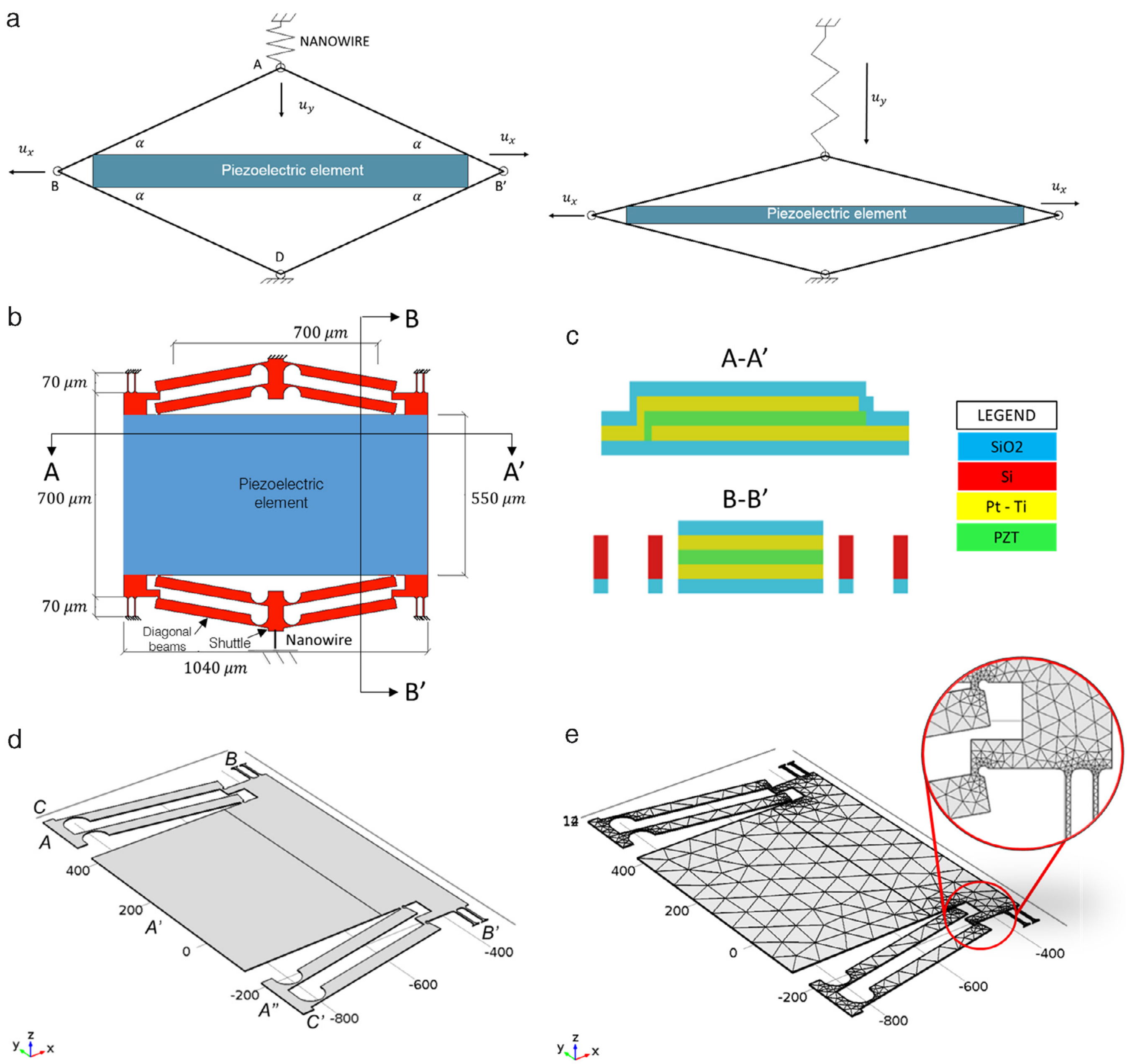

Fig. 4. (a) Scheme of the sagittal amplification of piezoelectric displacement. (b) Shape and components of the piezoelectric actuator. (c) Cross-sections of the piezoelectric actuator, showing the different layers used in the model (Refer Fig. 4(b)). (d) 3-D model used in FEM software to conduct the electro-mechanics simulation with piezoelectric coupling. (e) Meshed 3-D model showing the prism elements. Inset shows the hinges that connect the piezoelectric element with the diagonal beams.

applied in the z-direction to actuate the piezoelectric membrane; meaning an electric potential was applied between the top and bottom faces of the piezoelectric layer. Since the piezoelectric actuator is a composite of many thin layered structures with different thickness as shown in Fig. 4(c), prismatic elements were used for meshing. As shown in Fig. 4(e), the mesh was built as planar triangles on the top layer and then extruded in the z-direction. The piezoelectric actuator is meshed with prisms (Fig. 4(e)), to provide

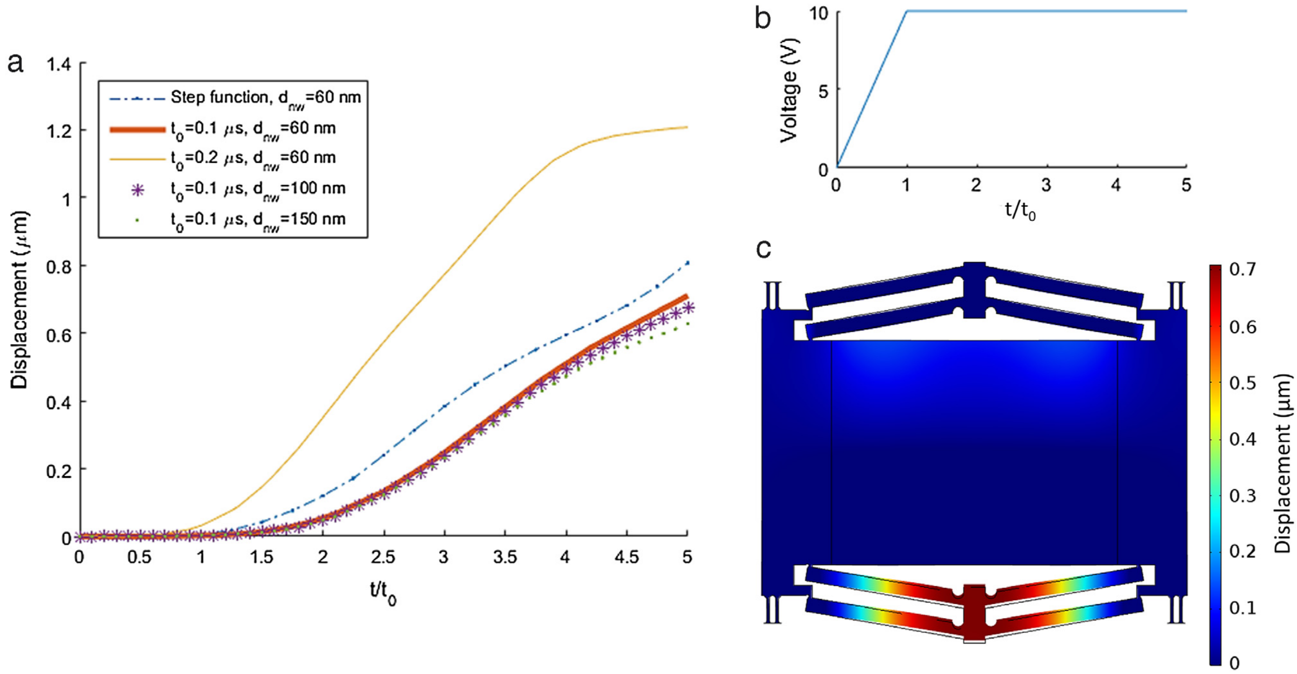

Fig. 5. (a) FEM simulation result showing the *y*-displacement of the piezoelectric MEMS with mechanical amplification as a function of voltage amplitude (shown in (b)) at different time scales (c) The displacement profile of the piezoelectric MEMS with amplification at an applied voltage of 10 V.

modeling flexibility and accurate results compared to other type of meshes for thin layered structures [49]. Also, since the hinges and beams had small cross-sections compared to the rest of the structure, the minimum length of the single element edge was reduced in the simulation. As such, a mesh with gradually varying element size was obtained, as the mesh transitions from larger structures to the small hinge parts in the structure. The stiffness of a silver nanowire with 100 nm diameter and 2 μm length, ∼326 N/m, was prescribed on the top part of the central shuttle, Fig. 4(b).

In order to compute the actuation speeds the piezoelectric actuator is capable of, a nonlinear dynamic analysis was performed. This electro-mechanical implicit problem was solved using the Newton–Raphson algorithm, taking into account the piezoelectric coupling. The dynamic analysis was conducted using FEM by applying the following voltage (V) history:

$$\begin{cases} V = 0 & t \le 0 \\ V = V_0 & t > 0 \end{cases} \tag{6}$$

The results of the shuttle displacement in the *y*-direction while attached to a nanowire with a diameter of 60 nm and when a voltage step function with amplitude of 10 V is applied on the piezoelectric actuator is shown in Fig. 5(a).

The same analysis was run again with a more realistic slower application of the voltage, a time-dependent linear function, viz.,

$$\begin{cases} V = V_0 \dfrac{t}{t_0} & t \le t_0 \\ V = V_0 & t > t_0 \end{cases} \tag{7}$$

This scenario is more realistic because of the finite power supply from the source. A ramping time $t_0 = 0.1$ ms and $t_0 = 0.2$ ms, to achieve the maximum applied voltage V_0 as representatively shown in Fig. 5(b) was used in the simulations. As seen from Fig. 5(a) and (c) a displacement of ∼650 nm is achieved for all the silver nanowires of varied diameters, which is sufficient to strain them elasticity even up to ∼ 32.5%, given a gage length of 2 μm at strain rates of ∼ 10^6/s.

The results showed that if the voltage is applied with a linear function, the dynamic response of the system is also linear. Thus, in order to conduct nanomechanical tests at different strain rates, only the time scale of the applied voltage needs to be modified, limited only by the first resonance mode at 1.07 MHz.

The fabrication process for such a piezoelectric MEMS device should focus on obtaining a piezoelectric element that is perfectly symmetric with respect of the *x*–*y* plane, in order to avoid out-of-plane bending of the device. While this might be challenging in practice, it is, in principle, possible [39,41]. As such, the fabrication and the experimental characterization of this piezoMEMS device are left for future work.

6. Conclusions

MD simulations have proven to be very useful in understanding deformation mechanisms and size effects in nanomaterials. However, quantitative prediction of material properties has been much less satisfactory. For example, metallic nanowires studied with different force fields showed significant variations in the quantitative predictions of yield and strength. In order to validate such force fields, ways to conduct nanomechanical experiments at high strain rates need to be explored. Using a combination of FEM simulations and experiments, two different MEMS actuators, namely thermal and piezoelectric were explored. Thermal actuator can be used for conducting experiments on nanomaterials up to a strain rate of 1/s. Beyond this, the system starts to lag due to inertia and unavoidable thermal transients. In order to increase the actuation speed even further, piezoelectric actuation is referenced. Using a combination of analytical calculations and finite element modeling, a PZT actuator was explored. The analysis shows that a sagittal amplification scheme can apply the required displacements and force to a typical metallic nanowire and deform it at ultra-high speeds of ∼1.2 m/s, an approximately six orders of magnitude increase in the actuation speeds achievable with a thermal actuator. In summary, we establish a pathway to nanomechanical testing at ultra-high strain rates, which will enable a direct comparison to MD simulations.

Associated Content

Acknowledgments

H.D. Espinosa gratefully acknowledges support from NSF through award No. DMR-1408901. The authors would like to thank Dr. Wei Gao for performing atomistic simulations on the bicrystalline nanowires with different force fields.

References

[1] A. Husain, et al., Nanowire-based very-high-frequency electromechanical resonator, Appl. Phys. Lett. 83 (6) (2003) 1240–1242.
[2] J. Andzane, et al., Two-terminal nanoelectromechanical devices based on germanium nanowires, Nano Lett. 9 (5) (2009) 1824–1829.
[3] O.Y. Loh, H.D. Espinosa, Nanoelectromechanical contact switches, Nature Nanotechnol. 7 (5) (2012) 283–295.
[4] D. Jariwala, T.J. Marks, M.C. Hersam, Mixed-dimensional van der Waals heterostructures, Nature Mater. (2016).
[5] T. Filleter, et al., Nucleation controlled distributed plasticity in penta twinned silver nanowires, Small 8 (19) (2012) 2986–2993.
[6] B. Peng, et al., Measurements of near-ultimate strength for multiwalled carbon nanotubes and irradiation-induced crosslinking improvements, Nature Nanotechnol. 3 (10) (2008) 626–631.
[7] B. Wu, A. Heidelberg, J.J. Boland, Mechanical properties of ultrahigh-strength gold nanowires, Nat. Mater. 4 (7) (2005) 525–529.
[8] X. Wei, et al., Plasticity and ductility in graphene oxide through a mechanochemically induced damage tolerance mechanism, Nat. Commun. 6 (2015).
[9] D. Jang, et al., Deformation mechanisms in nanotwinned metal nanopillars, Nature Nanotechnol. 7 (9) (2012) 594–601.
[10] R. Ramachandramoorthy, et al., High strain rate tensile testing of silver nanowires: Rate-dependent brittle-to-ductile transition, Nano Lett. 16 (1) (2015) 255–263.
[11] M. Haque, M. Saif, Application of MEMS force sensors for in situ mechanical characterization of nano-scale thin films in SEM and TEM, Sensors Actuators A 97 (2002) 239–245.
[12] A.T. Jennings, J. Li, J.R. Greer, Emergence of strain-rate sensitivity in Cu nanopillars: Transition from dislocation multiplication to dislocation nucleation, Acta Mater. 59 (14) (2011) 5627–5637.
[13] C. Peng, et al., Strain rate dependent mechanical properties in single crystal nickel nanowires, Appl. Phys. Lett. 102 (8) (2013) 083102.
[14] A. Voter, Embedded atom method potentials for seven fcc metals: Ni, Pd, Pt, Cu, Ag, Au, and Al. Los Alamos National Laboratory, Unclassified Technical Report No. LA-UR, 1993, pp. 93-3901.
[15] S. Foiles, M. Baskes, M.S. Daw, Embedded-atom-method functions for the fcc metals Cu, Ag, Au, Ni, Pd, Pt, and their alloys, Phys. Rev. B 33 (12) (1986) 7983.
[16] C. Deng, F. Sansoz, Fundamental differences in the plasticity of periodically twinned nanowires in Au, Ag, Al, Cu, Pb and Ni, Acta Mater. 57 (20) (2009) 6090–6101.
[17] J.A. Zimmerman, H. Gao, F.F. Abraham, Generalized stacking fault energies for embedded atom FCC metals, Modelling Simulation Mater. Sci. Eng. 8 (2) (2000) 103.
[18] C.R. Weinberger, W. Cai, Plasticity of metal nanowires, J. Mater. Chem. 22 (8) (2012) 3277–3292.
[19] S. Ryu, K. Kang, W. Cai, Predicting the dislocation nucleation rate as a function of temperature and stress, J. Mater. Res. 26 (18) (2011) 2335–2354.
[20] T. Zhu, et al., Temperature and strain-rate dependence of surface dislocation nucleation, Phys. Rev. Lett. 100 (2) (2008) 025502.
[21] P. Hänggi, P. Talkner, M. Borkovec, Reaction-rate theory: Fifty years after Kramers, Rev. Modern Phys. 62 (2) (1990) 251.
[22] A.F. Voter, Parallel replica method for dynamics of infrequent events, Phys. Rev. B 57 (22) (1998) R13985.
[23] C.R. Weinberger, G.J. Tucker, Multiscale Materials Modeling for Nanomechanics, vol. 245, Springer, 2016, p. 214.
[24] A.T. Jennings, et al., Modeling dislocation nucleation strengths in pristine metallic nanowires under experimental conditions, Acta Mater. 61 (6) (2013) 2244–2259.
[25] H. Sheng, et al., Highly optimized embedded-atom-method potentials for fourteen fcc metals, Phys. Rev. B 83 (13) (2011) 134118.
[26] P. Williams, Y. Mishin, J. Hamilton, An embedded-atom potential for the Cu–Ag system, Modelling Simulation Mater. Sci. Eng. 14 (5) (2006) 817.
[27] Y. Zhu, A. Corigliano, H.D. Espinosa, A thermal actuator for nanoscale in situ microscopy testing: Design and characterization, J. Micromech. Microeng. 16 (2) (2006) 242.
[28] R.A. Bernal, et al., Intrinsic Bauschinger effect and recoverable plasticity in pentatwinned silver nanowires tested in tension, Nano Lett. 15 (1) (2014) 139–146.
[29] P.M. Osterberg, S.D. Senturia, M-TEST: A test chip for MEMS material property measurement using electrostatically actuated test structures, J. Microelectromechanical Syst. 6 (2) (1997) 107–118.
[30] J.A. Wright, Y.-C. Tai, S.-C. Chang, A large-force, fully-integrated MEMS magnetic actuator, in: Solid State Sensors and Actuators, 1997, TRANSDUCERS'97 Chicago, 1997 International Conference on, IEEE, 1997.
[31] A. Corigliano, et al., Electro-thermal actuator for on-chip nanoscale tensile tests: analytical modelling and multi-physics simulations, Sens. Lett. 5 (3–1) (2007) 592–607.
[32] Y. Zhu, H.D. Espinosa, An electromechanical material testing system for in situ electron microscopy and applications, Proc. Natl. Acad. Sci. USA 102 (41) (2005) 14503–14508.
[33] Y. Zhu, N. Moldovan, H.D. Espinosa, A microelectromechanical load sensor for in situ electron and x-ray microscopy tensile testing of nanostructures, Appl. Phys. Lett. 86 (1) (2005) 013506.
[34] E. Hosseinian, O.N. Pierron, Quantitative in situ TEM tensile fatigue testing on nanocrystalline metallic ultrathin films, Nanoscale 5 (24) (2013) 12532–12541.
[35] A. Corigliano, L. Domenella, G. Langfelder, On-chip mechanical characterization using an electro-thermo-mechanical actuator, Exp. Mech. 50 (6) (2010) 695–707.
[36] H.D. Espinosa, Y. Zhu, N. Moldovan, Design and operation of a MEMS-based material testing system for nanomechanical characterization, J. Microelectromech. Syst. 16 (5) (2007) 1219–1231.
[37] H. Loebl, et al., Piezoelectric thin AlN films for bulk acoustic wave (BAW) resonators, Mater. Chem. Phys. 79 (2) (2003) 143–146.
[38] M. Rinaldi, C. Zuniga, G. Piazza, 5-10 GHz AlN contour-mode nanoelectromechanical resonators, in: Micro Electro Mechanical Systems, 2009, MEMS 2009, IEEE 22nd International Conference on, IEEE, 2009.
[39] S. Trolier-McKinstry, P. Muralt, Thin film piezoelectrics for MEMS, J. Electroceram. 12 (1–2) (2004) 7–17.
[40] N.J. Conway, S.-G. Kim, Large-strain, piezoelectric, in-plane micro-actuator, in: Micro Electro Mechanical Systems, 2004, 17th IEEE International Conference on(MEMS), IEEE, 2004.
[41] L.-P. Wang, et al., Design, fabrication, and measurement of high-sensitivity piezoelectric microelectromechanical systems accelerometers, J. Microelectromechanical Syst. 12 (4) (2003) 433–439.
[42] N.J. Conway, Z.J. Traina, S.-G. Kim, A strain amplifying piezoelectric MEMS actuator, J. Micromech. Microeng. 17 (4) (2007) 781.
[43] C. Giordano, et al., AlN on polysilicon piezoelectric cantilevers for sensors/actuators, Microelectron. Eng. 86 (4) (2009) 1204–1207.
[44] H.K. Kommepalli, et al., Design, fabrication, and performance of a piezoelectric uniflex microactuator, J. Microelectromech. Syst. 18 (3) (2009) 616–625.
[45] H. Kim, S. Priya, K. Uchino, Modeling of piezoelectric energy harvesting using cymbal transducers, Jpn. J. Appl. Phys. 45 (7R) (2006) 5836.
[46] K. Onitsuka, et al., Metal-ceramic composite transducer, the "Moonie", J. Intell. Mater. Syst. Struct. 6 (4) (1995) 447–455.
[47] J. Zhang, et al., A miniature class V flextensional cymbal transducer with directional beam patterns: The double-driver, Ultrasonics 39 (2) (2001) 91–95.
[48] Z.J. Traina, A Large Strain Piezoelectric Microactuator By Folding Assembly, MSc Thesis, Massachusetts Institute of Technology, 2007, pp. 22–37.
[49] E. Abenius, F. Edelvik, Thin sheet modeling using shell elements in the finite-element time-domain method, IEEE Trans. Antennas Propag. 54 (1) (2006) 28–34.